Brick geometry revisited – with a slant

Gijs J.O. Vermeer, *3DSymSam*, July 2016

Introduction

Brick geometry (or brick-wall geometry) in which the shots are staggered or "bricked" used to be quite popular in the early days of 3D seismic land data acquisition. The main reason was that the largest minimum offset (LMOS) of a brick geometry is smaller than that of an orthogonal geometry with continuously sampled shot lines. Another reason was that the stack response of narrow acquisition geometries is better for brick geometry than for regular geometry (Vermeer, 1998). The latter reason has vanished with the almost universal introduction of wide geometries in recent years, whereas the main reason remains, albeit that it has become less important with the use of smaller line intervals.

From the earliest days of promoting 3D symmetric sampling I have stressed the importance of spatial continuity (Vermeer, 1994) and the need to minimize spatial discontinuities in the acquisition geometries. Therefore, I discouraged the use of brick geometries: "If staggered shot lines are used (as in brick-wall geometry), the shot lines are only partially sampled, leading to cross-spreads that are split into a number of strips. The number of edges in this geometry is much larger than in the continuous shot-line geometry; spatial continuity in this geometry is therefore degraded." (Vermeer, 1998, p. 1636). Perhaps this contributed to less use of brick geometry. Anyway, in recent years only a few case studies have been published in which the seismic data were acquired using brick geometry. Jianming et al. (2009) report a successful fracture-detection and -orientation analysis based on data acquired with brick geometry. Konyushenko et al. (2014) discuss the imaging of a wide-azimuth brick geometry.

Users of brick geometry, aware of the negative aspects of discontinuous shot lines, have often turned to slanted geometry as a better alternative. The crossline interval between shots is kept the same as in the corresponding orthogonal or brick geometry to ensure square bins (although not all midpoints are now centered in the bins). Common choices for the angle of the shot line with the receiver line are 71.6 and 63.4 degrees; 71.6° requires that all receiver spreads move one station in the inline direction every third shot, whereas 63.4° requires a one-station move every other shot. Moving the spreads ensures that all shots remain center-spread as much as possible. In case the angle is 45° all spreads are moved one receiver station with each next shot; in this case all midpoints are centered in the bins. Slanted geometry is more often used than brick geometry, usually with 45° between shot and receiver lines. Karagül et al. (2004) used slanted geometry with a 63.4° angle.

The main reason to look again at brick geometry is the observation that brick geometry is suitable for offset-vector tile (OVT) analysis, and the question is whether or not this should lead to a rehabilitation of brick geometry. Another reason is to show that the difference in the LMOS of brick versus orthogonal is not as large as stated in Vermeer (1998).

The first part of this paper discusses brick geometry. It starts with a discussion of LMOS. Next I describe OVT gathers, including reciprocal OVT gathers, followed by some simple imaging analysis of those gathers. The second part investigates slanted geometry. In a discussion the results for brick geometry are compared with those of slanted and orthogonal geometry and pros and cons of using brick geometry or slanted geometry are revisited.

Brick geometry is a type of orthogonal geometry with partially sampled shot lines. Yet, in this paper, orthogonal geometry with fully sampled shot lines is just referred to as "orthogonal geometry".

Brick geometry

Largest minimum offset (LMOS)

An important property of brick geometry is that its LMOS is smaller than the LMOS of orthogonal geometry. This means that continuous coverage (in each bin at least one trace with data that are not muted) is reached at shallower levels for brick geometry than for orthogonal geometry. However, the difference in LMOS is not as large as originally assumed in Vermeer (1998). An analysis in Appendix A shows that for brick geometry LMOS = 1.25 RLI, rather than √(1.25) RLI (assuming SLI = RLI). The difference is illustrated in Figure 1b, where the shot-receiver pair on the right has the smaller offset, whereas the actual LMOS is represented by the shot-receiver pair on the left. Instead of 26% difference in LMOS between orthogonal and brick geometry, the difference is only 13%. LMOS for orthogonal geometry is illustrated in Figure 1a.

In practice, LMOS not only depends on the line intervals but also on the shot and receiver sampling intervals along the lines. The best approximation of the LMOS given by above formulas is for very small sampling intervals. The fold maps of Figure 2 illustrate for geometries with line intervals of 400 m and sampling intervals of 50 m the difference in LMOS between the two geometries and for which bins LMOS applies. Note that LMOS for the brick geometry occurs in a midpoint that is off-center similar as LMOS in Figure 1b. It may also be observed that orthogonal geometry requires many more bins with twofold data to reach at least singlefold coverage in all bins than brick geometry (number of green bins in each unit cell). The difference in LMOS between brick and orthogonal geometry for this sampled situation is 11%.

OVTs in regular brick geometry

Figure 3 illustrates the point made in the introduction that the cross-spread (all data acquired with receivers in a single receiver line listening to the shots in a single shot line) in brick geometry consists of a number of narrow strips with height equal to RLI/2. As a consequence there is less spatial continuity in brick geometry than in orthogonal geometry in which each cross-spread constitutes a single continuous midpoint area.

Even though the cross-spreads in regular brick geometry are broken up, the fullfold area of the geometry has constant fold just as a regular orthogonal geometry. This is illustrated in Figure 4a for a 36-fold orthogonal geometry on the left and a 36-fold brick geometry on the right. The pink area corresponds to all bins with a fold of 36. The fullfold area of brick geometry is smaller than for the equivalent orthogonal geometry (geometry with the same shot intervals, receiver intervals, RLI, SLI, maximum inline offset, and maximum crossline offset). In this brick geometry the inline distance required to build to full fold equals 1100 m, whereas in the equivalent orthogonal geometry it is 1000 m.

OMNI 3D may be used to extract singlefold OVT gathers from an orthogonal geometry by the specification of a range 2 * SLI of inline offsets and a range 2 * RLI of crossline offsets. The same procedure produces singlefold gathers for the brick geometry of Figure 4a. Figure 4b shows midpoint coverage for shortest offsets [inline and crossline offsets both ranging (-400 – 400 m)], and Figure 4c for a range of long offsets. Figure 4b shows that the short offsets give singlefold coverage in the whole survey area of orthogonal geometry, whereas brick geometry shows irregular coverage along the edges of the survey area. Figure 4c (long offsets from the upper-right corner of the cross-spread, cf. Figure 5) shows one trace in each bin in and around the fullfold area of the geometry. Again, the only apparent difference between orthogonal and brick geometry is the presence of some irregularities along the edges of the OVT-coverage.

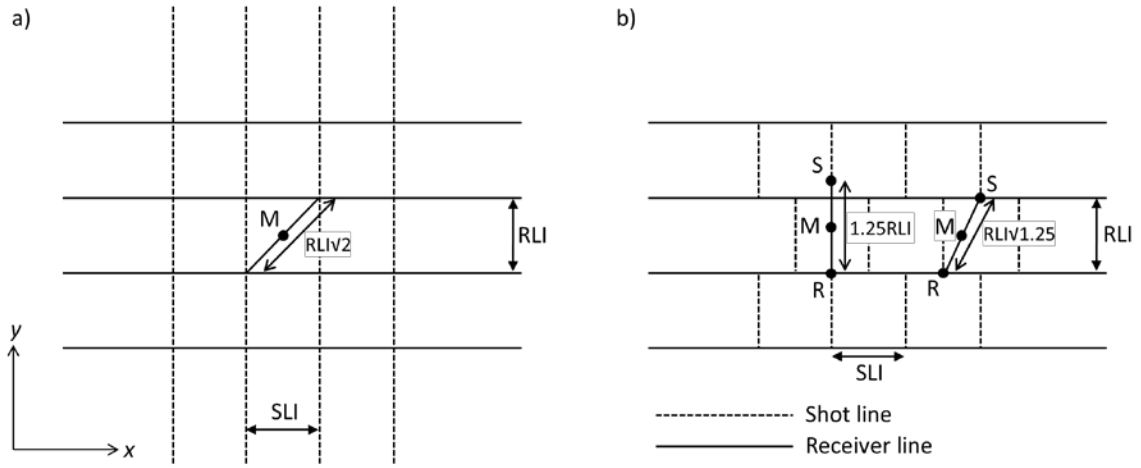

Fig. 1. Comparison of LMOS for (a) orthogonal geometry and (b) brick-wall geometry. For equivalent geometries and for SLI = RLI, LMOS = RLI √2 in (a) and LMOS = 1.25 RLI in (b). Earlier it was assumed incorrectly that LMOS = RLI √1.25 (situation on the right of (b)).

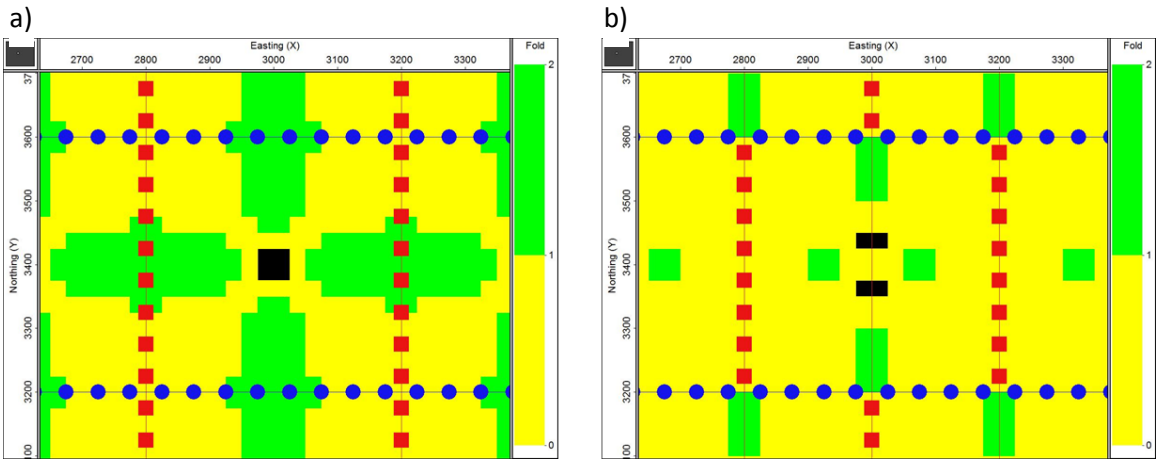

Fig. 2. Fold maps for (a) regular and (b) brick geometry for all absolute offsets just smaller than LMOS. In (a) LMOS = 530.3 m, in (b) LMOS = 475.7 m. The black bins are empty and correspond to bins with LMOS. Line intervals are 400 m; sampling intervals are 50 m.

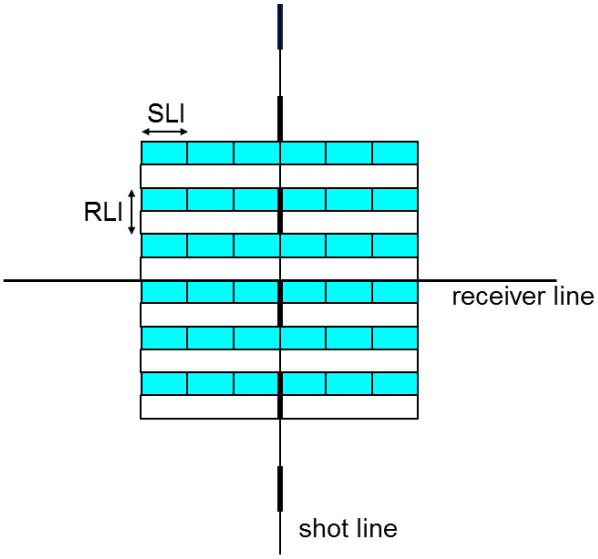

Fig. 3. Cross-spread in brick geometry consists of narrow strips of coverage alternating with narrow empty strips.

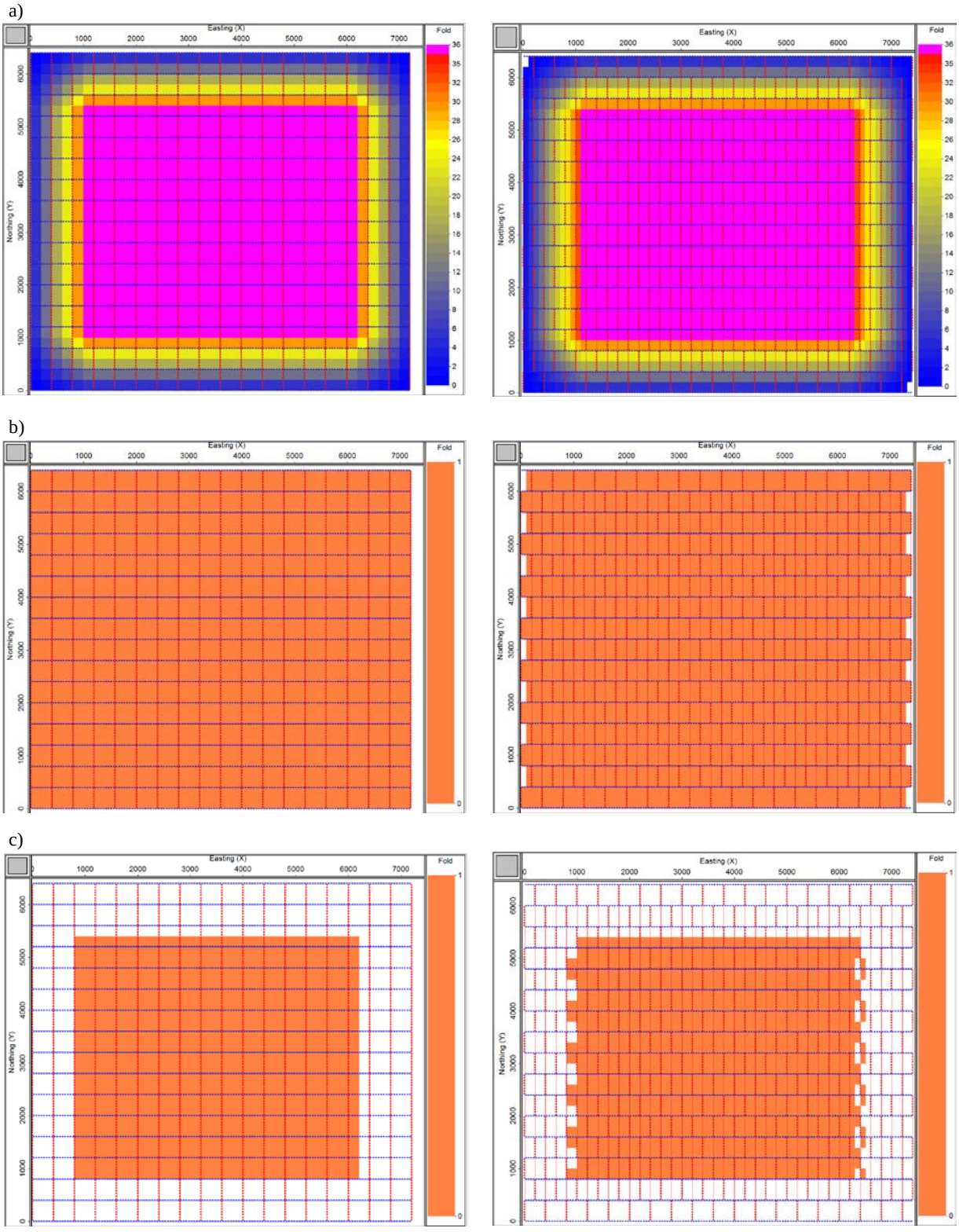

Fig. 4. Comparison of OVT-analysis of orthogonal geometry (left column) with brick geometry (right column). (a) Fold map of the two geometries, note that the fullfold area of orthogonal geometry starts at 2.5 SLI from the survey edge, whereas it starts at 2.75 SLI from the survey edge in brick geometry, (b) shortest offsets OVT gather for inline offsets -400 – 400 m and crossline offsets -400 – 400 m, the absolute offsets in these displays range from nearly zero to 400v2, (c) OVT gathers for inline offsets 1600 – 2400 m and crossline offsets -2400 — -1600 m.

Yet, there are bigger differences between the OVT gathers of orthogonal and brick geometry. Figure 5 compares OVTs for orthogonal geometry (Figure 5a) and brick geometry (Figure 5b and 5c). Figure 5a-left illustrates that the midpoint area of a cross-spread is continuous. The only discontinuities are the edges of the cross-spread. In this example the midpoint area of the cross-spread can be split into 36 OVTs, each of which is also continuous. The OVTs in the upper-right corner and in the lower-left corner are highlighted. These two OVTs are called reciprocal to each other: they cover the same range of absolute offsets and their azimuth range differs 180°. Figure 5a-right shows the situation that a pair of reciprocal OVTs cover the same midpoint range. Interestingly, the shots of one OVT form a big + sign together with the receivers of the other OVT (see also Vermeer, 2012, Fig. 2.32b).

Despite the constant fold of the OVT gathers of brick geometry (Figures 4b-right and 4c-right), these gathers cannot be composed of OVTs with size RLI x SLI, because only narrow strips of midpoints are gathered in brick geometry as illustrated in Figure 3. Hence, an area with size RLI x SLI must consist of contributions from different cross-spreads. Figures 5b and 5c illustrate two different ways of creating RLI x SLI sized areas which comprise all shot-receiver pairs corresponding to the upper-right OVT in a cross-spread of orthogonal geometry.

The central shot line in Figure 5b-left contributes the upper strip in the OVT-sized area, whereas the two other shot lines each contribute a quarter OVT area. Note that the left quarter contains larger inline offsets than the right quarter. As a consequence there is a spatial discontinuity in the vector offsets between the upper and the lower part of the OVT-sized area. Figure 5b-right shows that shots and receivers of overlapping reciprocal vector offset ranges are no longer composed of simple crosses as in Figure 5a-right. Instead, 6 shot lines contribute to the required range of offset vectors.

Rather than using extra shot lines, Figure 5c shows that also extra receiver lines can be selected to gather all required shot-receiver pairs in an OVT-sized area. In Figure 5c-left the same shot interval is used to create adjacent strips of coverage using two adjacent receiver lines. Again, there is a spatial discontinuity between the two strips as the upper strip has smaller crossline offsets than the lower strip. The overlapping reciprocal OVT can only be constructed by using two shot lines shooting into two short pieces of receiver line (Figure 5c-right). The pattern of contributing shots and receivers now uses four receiver lines and three shot lines.

The OVTs and also the reciprocal OVTs of Figures 5b and 5c can be repeated in the inline direction to give singlefold coverage in a long strip across the survey area. However, in the crossline direction they can only be repeated by moving half a shot-line interval to the right or to the left. This means that these OVTs are staggered with respect to each other in the same way as the shot lines are staggered.

The discussion of Figure 5 shows that the regular coverage of the OVT gathers of brick geometry as illustrated in Figure 4b-right and 4c-right is only part of the story. Orthogonal geometry has larger continuous tiles than brick geometry, whereas the pairs of reciprocal tiles in brick geometry are composed in a more complex way from the shot and receiver lines. The effect of these differences on imaging is discussed next.

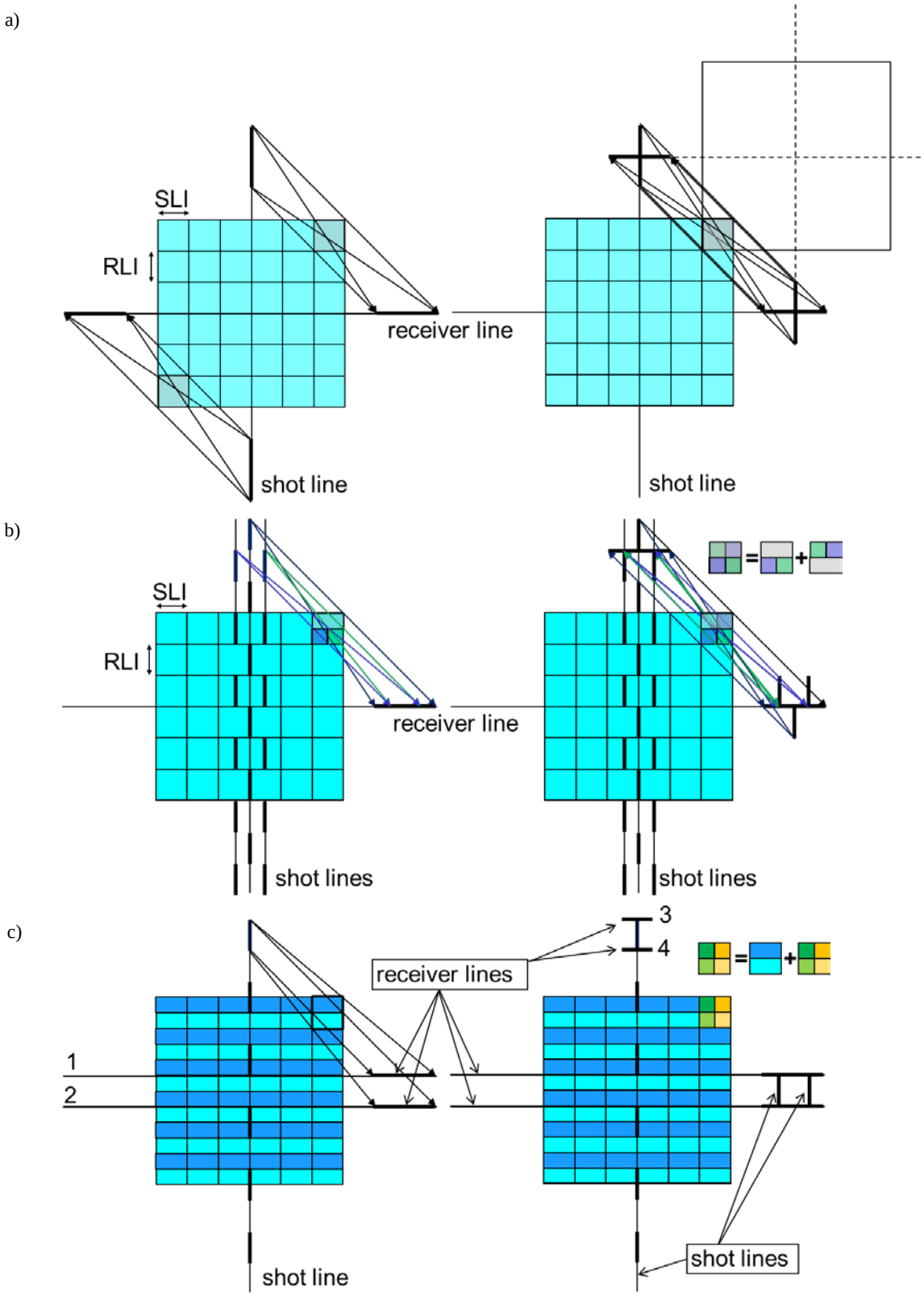

Fig. 5. OVTs in orthogonal geometry and in brick geometry. Left: construction of upper-right OVT, right: construction of pair of reciprocal OVTs. (a) Orthogonal geometry; reciprocal OVTs are formed by two crosses, each consisting of a piece of receiver line and a piece of shot line.(b) OVT-construction in brick geometry using three shot lines. Now a pair of reciprocal OVTs is constructed from receivers along two receiver lines and from shots along 6 shot lines. (c) OVT construction in brick geometry using two receiver lines. Now a pair of reciprocal OVTs is constructed from receivers along four receiver lines and from shots along three shot lines.

Comparison of OVT imaging between orthogonal and brick geometry

Over the last ten years the use of OVT gathers (elsewhere also called COV gathers) has become increasingly important in velocity-model building, anisotropy analysis, imaging, and other processing steps. It would be ideal to have true COV gathers (i.e., all offset vectors exactly the same) as input for most of those steps, but the OVT gathers represent the best approximation to true COV gathers for any regular acquisition geometry. Smaller line intervals in orthogonal geometry or smaller separation of receivers in areal geometry increase the usefulness of the OVT gathers. In the following imaging tests I use the brick geometry described in Figure 3a and the equivalent orthogonal geometry. The geometries have rather large 400-m line intervals.

The model used for the tests consists of an interface dipping 15° to the West in a 3000 m/s constant velocity medium. The depth of the interface is 3000 m at Easting-Northing coordinates (3600, 3000). Figure 6 shows the results of imaging the orthogonal geometry on the left and the brick geometry on the right. Figures 6a and 6b show results for singlefold data and Figures 6c and 6d for twofold data. It is important to realize that each 400 x 400 m area contains exactly the same collection of shot-receiver pairs, but their distribution inside each area differs between the orthogonal and brick geometry.

Figure 6a shows the imaged horizon slices for the OVT in the upper-right corner of the cross-spread (see Figure 5). The inline offset range is 1600 – 2400 m and the crossline offset range is -2400 – -1600 m. Figure 6b shows the results for the OVT on the opposite side of the cross-spread with inline offsets -2400 – -1600 m and crossline offsets 1600 – 2400 m. The ideal imaging result would show constant amplitude in both cases. Instead there is considerable amplitude variation (acquisition footprint) for both geometries, but this variation is larger for orthogonal than for brick geometry. This result can be explained by the fact that in brick geometry there are more yet smaller spatial discontinuities than in orthogonal geometry. This observation applies in particular to the crossline offsets: in orthogonal geometry the spatial discontinuity shows jumps of 800 m, whereas in brick geometry the jumps are only 400 m.

Figures 6c and 6d show the imaged horizon slices for the combined OVTs in the upper-right and the lower-left corners of the cross-spread. The range of the amplitude scale in Figure 6c is twice the scales in Figures 6a and 6b in an attempt to balance the effect of having twice as many input traces in Figure 6c. In Figure 6d the amplitude scale is just large enough to encompass all amplitudes of the result for the brick geometry. Now the result for orthogonal geometry is much better than for brick geometry. Inspection of Figures 6a and 6b shows why summing two results has such a different effect between the two geometries. For orthogonal geometry the red amplitudes in Figure 6a coincide with the blue amplitudes in Figure 6b. On the other hand, for brick geometry reds in Figure 6a tend to coincide with reds in Figure 6b. The underlying cause of these differences can be understood by inspection in Figure 5 of the shot-receiver pairs that contribute to the reciprocal tiles. In orthogonal geometry (Figure 5a) the same midpoint area is covered by two pairs of shot and receiver ranges that are maximally different. As a result subsurface illumination is maximally different as well to the extent that illumination gaps and overlaps by the upper-right tile correspond to illumination overlaps and gaps by the lower-left tile. They mitigate each other's illumination irregularities. In brick geometry illumination with the small strips of midpoint coverage is much more erratic.

A thorough analysis of illumination with orthogonal geometry is discussed and shown in Vermeer (2012, p. 285-286). I did not make a similar analysis for brick geometry, but the staggered pattern of shooting combined with the narrow continuous strips must give a more erratic illumination pattern without substantial mitigating effects, if any.

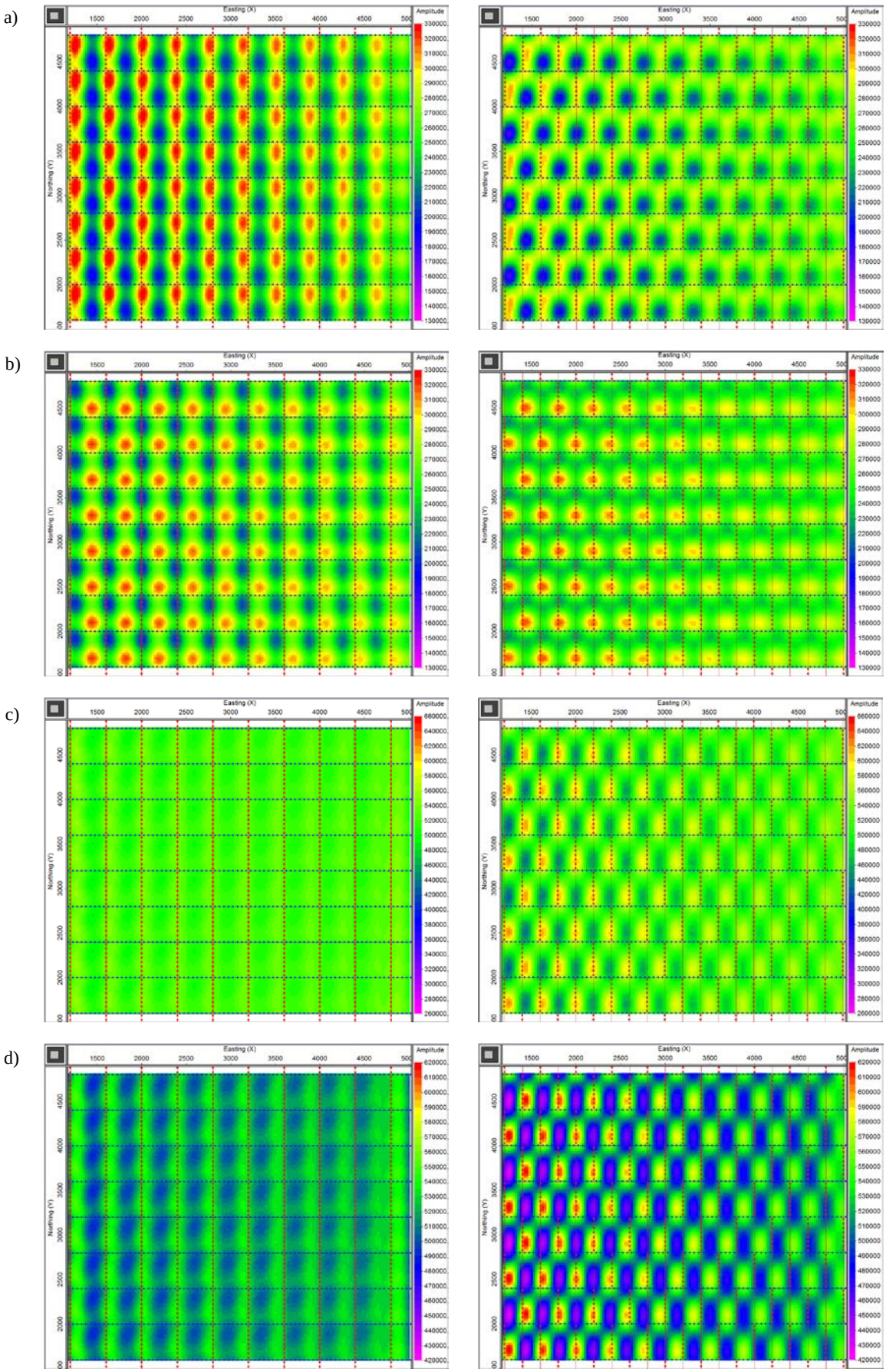

Fig. 6. Imaging comparisons between orthogonal (left) and brick (right) geometry using horizon slices of OVT gathers. (a) Upper-right OVTs, (b) Lower-left OVTs, (c) Reciprocal OVTs, upper right + lower left, (d) as (c) with amplitude scale just covering all brick amplitudes.

Slanted geometry

In this part of the paper the slanted geometry is equivalent with the orthogonal geometry and with the brick geometry that are discussed in the first part.

LMOS in slanted geometry

The shot lines of the slanted geometry being considered here make an angle α of 63.4 degrees with the receiver lines [tan (α) = 2]. Appendix B discusses the determination of LMOS in this geometry (with RLI = SLI, where SLI is defined as the inline distance between two neighboring shot lines). Figure 7a shows the result of this determination: three slanted spreads share a midpoint with the same absolute

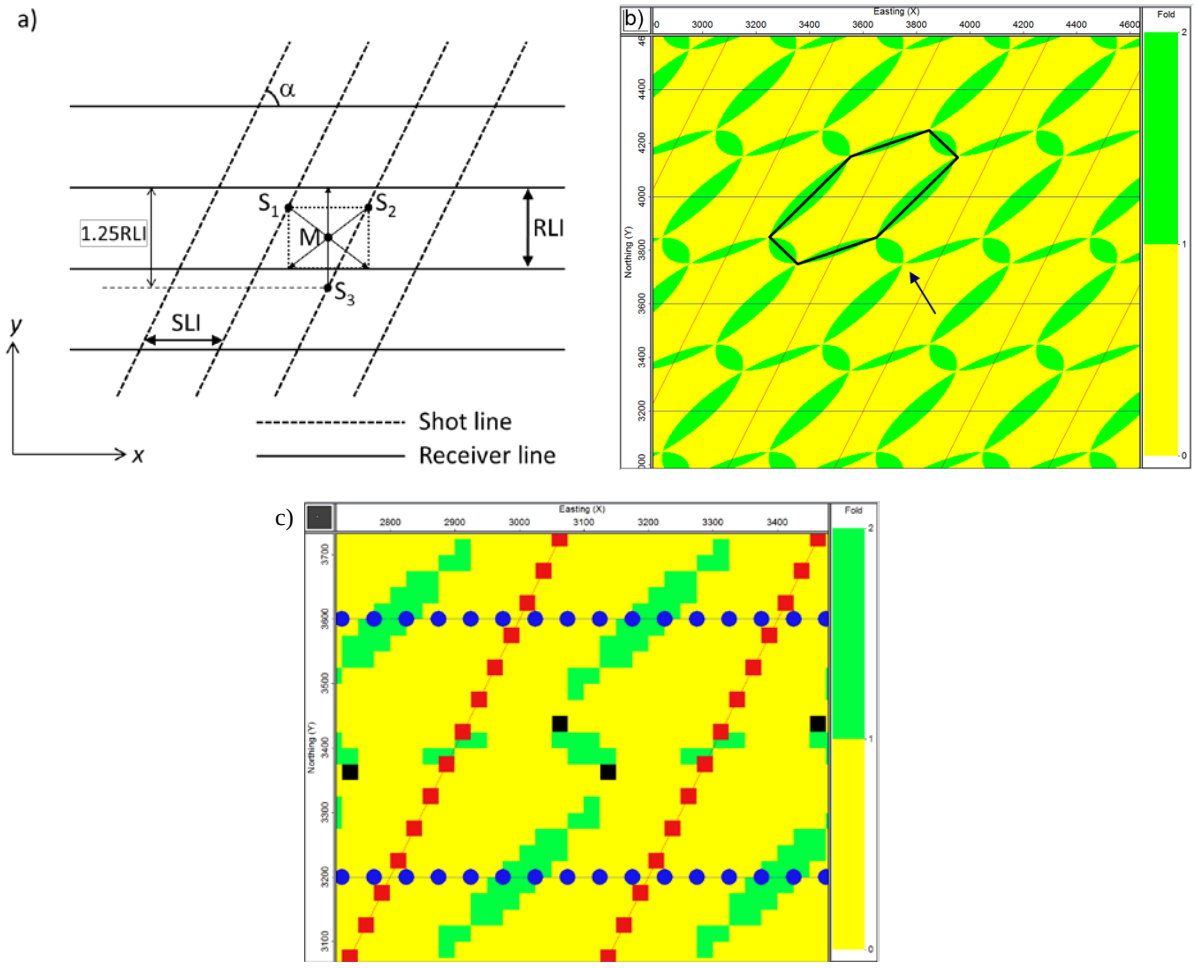

Fig. 7. LMOS in slanted geometry. (a) At midpoint M three slanted spreads possess a shot/receiver pair with exactly the same absolute offset. LMOS in this slanted geometry equals 1.25 RLI, same formula as for the brick geometry. (b) Fold map of slanted geometry for all offsets < 497.55 m. Line intervals in this example are 400 m, whereas station intervals are 5 m. The locus of all midpoints sharing the same absolute offset is an ellipse in slanted geometry. The arrow points at a position where three ellipses meet. This point corresponds to midpoint M in (a). For hexagon see Discussion: LMOS. (c) Fold map in equivalent slanted geometry for all offsets < 476.4 m. The black bins are empty and correspond to bins with LMOS = 476. 5m. Compare with Figure 2.

offset. This offset is the LMOS of this geometry. Figure 7b illustrates the fold map for all absolute offsets < 497.55 m. The theoretical value of LMOS is 1.25 RLI = 500 m; in Figure 7b the station intervals are very small so that the actual value of LMOS is very close to the theoretical value for infinitely small station intervals. Figure 7c shows the fold map for slanted geometry with 50-m station intervals. Now LMOS = 476.5 m, nearly the same as for the equivalent brick geometry (see Figure 2).

The beauty of this slanted geometry is that it has the same LMOS as the equivalent brick geometry, whereas the shot lines are now continuous.

OVTs in slanted geometry

Figure 8 illustrates that the midpoint area of a slanted spread has a diamond shape that is even more skewed than the shot lines; this extra skew is caused by moving the receiver spread with one station for every other shot along the shot line. As a consequence, also the OVTs are strongly skewed. Also, the continuous area of each OVT extends across a wider range of midpoints than in the equivalent orthogonal geometry

Figure 9 illustrates for slanted geometry what Figure 4 illustrates for orthogonal and brick geometry. The fullfold area of slanted geometry (Figure 9a) has jagged right and left edges. Also the edges of the shortest-offsets OVT gather (Figure 9b) and of the long-offset OVT gather (Figure 9c) are strongly jagged. Yet, in the crossline direction there are now only discontinuities between OVTs (every RLI), unlike in the brick geometry where there are spatial discontinuities every RLI/2.

Reciprocal offset-vector tiles are again formed by crosses consisting of a short piece of shot line and a short piece of receiver line, similar as shown in Figure 5a-right for orthogonal geometry. However, for slanted geometry the crosses are not square but skewed.

OVT imaging with slanted geometry

For the same model as used before for orthogonal and brick geometry, Figure 10 shows the horizon slices. Figure 10a and 10b show the result of imaging singlefold OVT gathers for the upper-right corner and lower-left corner of the slanted spread, respectively. The input to Figure 10a consists of the same range of offsets and azimuths as used as input to Figure 6a, and Figure 10b corresponds to Figure 6b.

Figures 10c and 10d show the result of twofold imaging: the sum of the upper-right and lower-left corners with the same amplitude scales as used in Figures 6c and 6d, respectively. Because the highs and lows in Figure 10a do not correspond to the lows and highs in Figure 10b, their sum still shows considerable variation in amplitude, although not as much as the corresponding result for brick geometry (Figure 6c-right and 6d-right).

Discussion

To come to a final conclusion on the relative merits of orthogonal, brick and slanted geometries, I discuss the following aspects

1. LMOS,
2. Imaging,
3. Suitability for prestack noise removal, and
4. Efficiency

LMOS

LMOS determines the shallowest level where the stack has nonzero values. The larger LMOS the larger the time where there is at least singlefold coverage. Brick geometry and slanted geometry provide shallower coverage than orthogonal geometry for the same line intervals and the same sampling intervals.

Figures 4b and 9b show singlefold coverage for the same range of inline and crossline offsets centered around zero offset and with maximum offset equal to RLI √2 (LMOS in orthogonal geometry). Yet, the fact that LMOS is smaller in brick and in slanted geometry than in orthogonal geometry means that

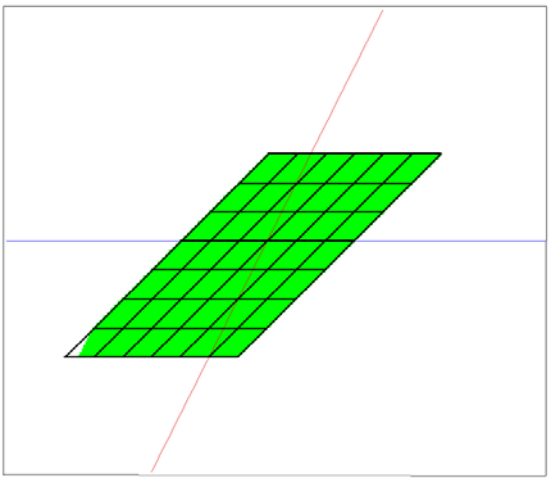

Fig. 8. Slanted spread with OVTs. Each OVT has a diamond shape and extends across a larger range of midpoints than equivalent OVTs in orthogonal geometry.

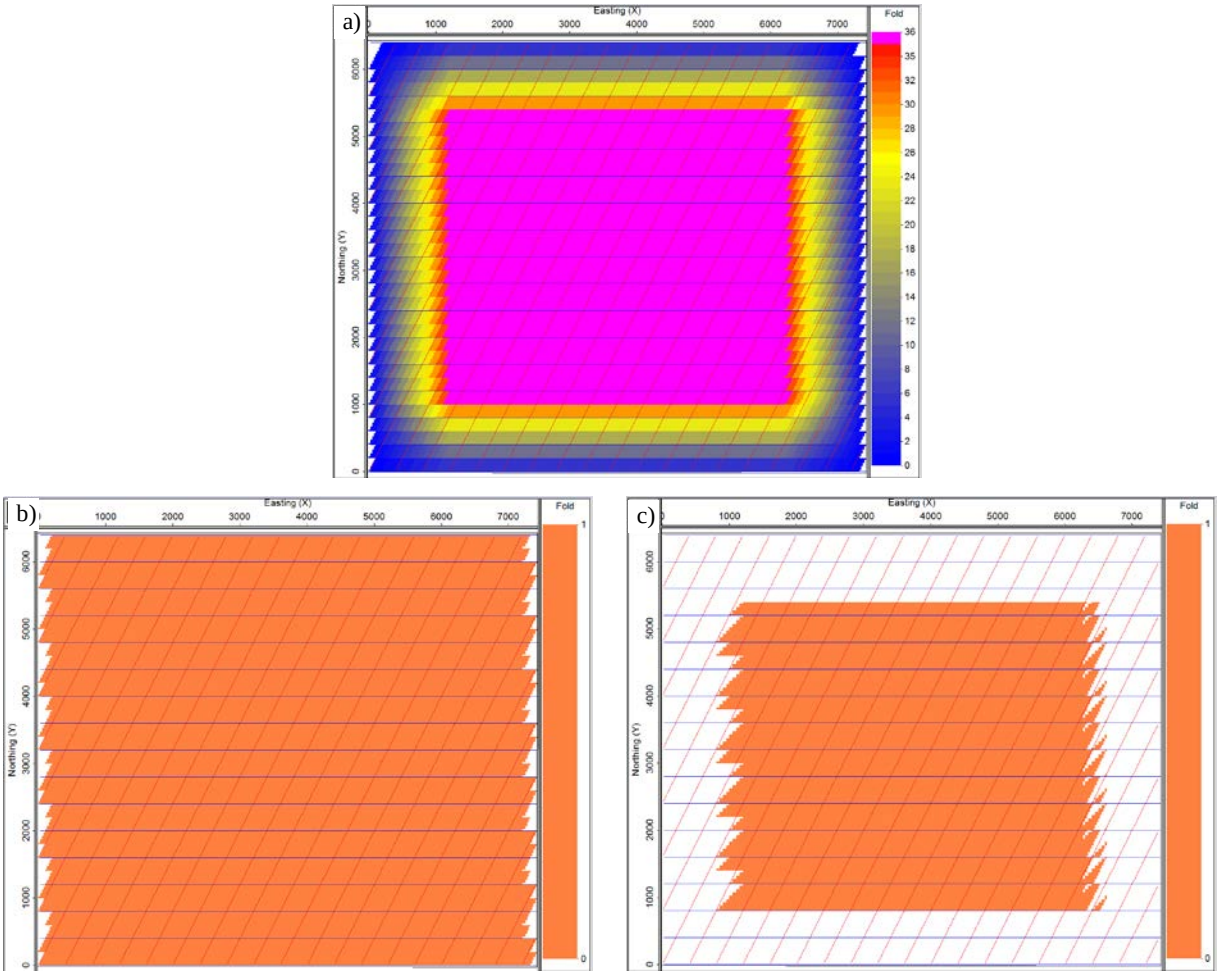

Fig. 9. OVT-analysis of slanted geometry. (a) Fold map of example geometry, (b)) shortest offsets OVT gather for inline offsets -400 – 400 m and crossline offsets -400 – 400 m, the absolute offsets in this display range from nearly zero to 400√2, (c) OVT gather for inline offsets 1600 – 2400 m and crossline offsets -2400 — -1600 m.

there must also be a complete singlefold coverage in brick and in slanted geometry for a smaller range of offsets, just up to LMOS. For slanted geometry this can be seen easily in Figure 7b. Selecting from each slanted spread only the midpoints inside a hexagon as indicated also provides single coverage,

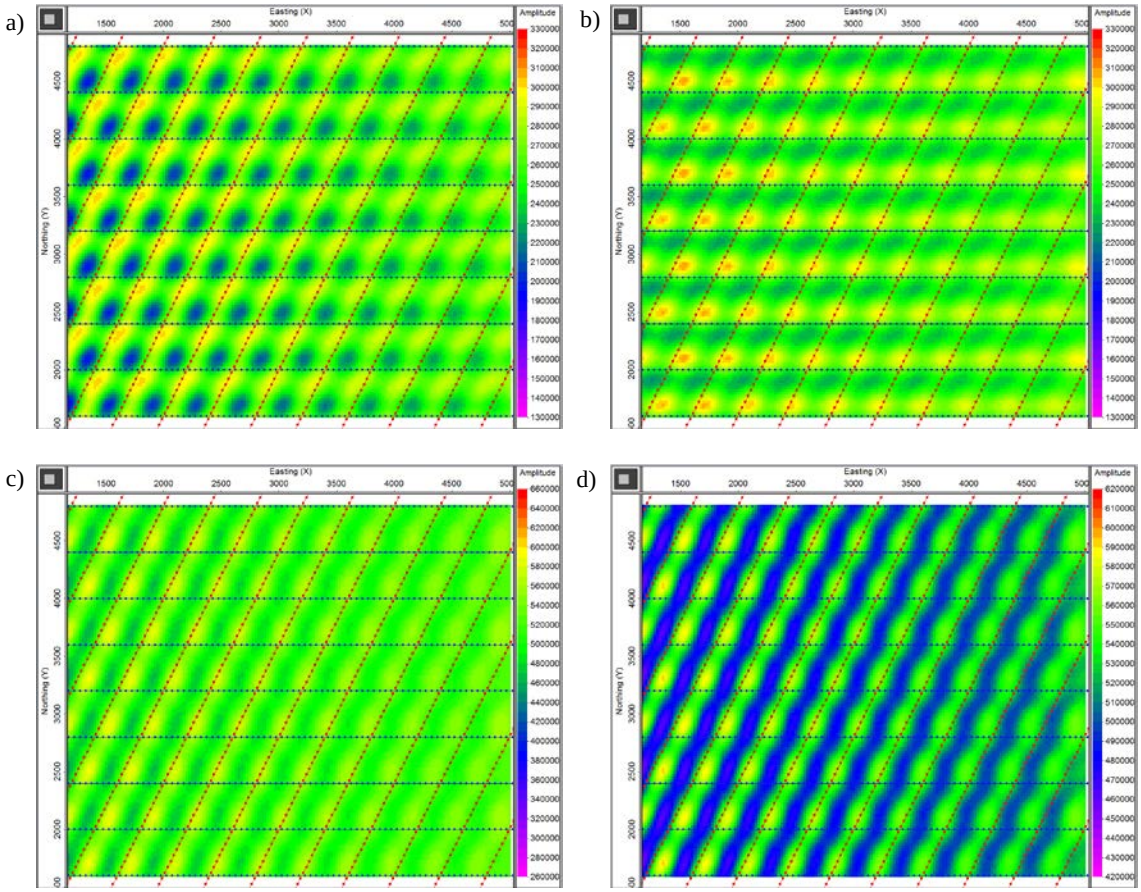

Fig. 10. Horizon slices for OVT gathers of slanted geometry. (a) Upper-right OVT, (b) Lower-left OVT, (c) Reciprocal OVT, upper right + lower left, (d) as (c) with amplitude scale as in Figure 6d. Compare with Figure 6.

but now with maximum offset equal to LMOS of the slanted geometry. In practice, this can be achieved by just selecting in each midpoint the smallest absolute offset.

A smaller LMOS is particularly important for data acquisition with large line intervals; yet, it should be realized that imaging of shallow data requires in general especially small station intervals due to the slow velocities. 50-m sampling as in my examples is not normally good enough. Smaller line intervals also lead to shallower coverage and this route is taken more often nowadays.

Imaging

In orthogonal geometry each OVT consists of a continuous area of data taken from a single cross-spread. A tiling of OVTs in an OVT gather features spatial discontinuities along the edges of each tile. When imaging an OVT gather the data required to create an image will often extend across more than one tile. This phenomenon is nicely illustrated in Vermeer (2012, Fig. 10.17e). The spatial discontinuities across edges affect the quality of the image and may lead to acquisition footprints as shown in Figures 6a-left and 6b-left. In brick geometry there are more spatial discontinuities but they are smaller. As a consequence, Figures 6a-right and 6b-right show an acquisition footprint that is less serious than for orthogonal geometry.

This difference between orthogonal and brick geometry changes drastically when combining reciprocal OVT gathers as done in Figure 6c. The arrangement of shots and receivers illustrated in Figure 5 ensures that the two gathers are very much complementary leading to a substantial reduction in acquisition footprint. For brick geometry there is much less reduction in footprint when combining the two OVT gathers. Comparison of Figure 10 with Figure 4 shows that twofold imaging with reciprocal OVT gathers

in slanted geometry is not as good as in orthogonal geometry but better than in brick geometry. This result emphasizes the benefit of continuous shot lines.

Suitability for prestack noise removal

The difference between properties of coherent noise and desired signal can be optimally exploited in cross-spreads and in slanted spreads because the events themselves are continuous throughout the spreads. Three-dimensional filtering can be applied in those spreads leading to clean output results. A nice example for slanted spreads is shown in Karagül et al., (2004) and is reproduced in Vermeer (2012, Fig. 2.39). In brick geometry coherent events are only coherent in small ranges and it is much more difficult to exploit such coherency.

Efficiency

For equivalent parameters, brick geometry requires twice as many shot lines as orthogonal geometry. In areas where lines have to be cleared or otherwise be readied this difference involves considerably more effort, hence cost, if only because of the extra distance to be traveled from one brick to the next.

For equivalent parameters, slanted geometry requires clearing and readying of longer shot lines. The difference with orthogonal geometry is 12%. If there is no clearing or readying to be done it still requires traveling the extra distance.

For the same survey area orthogonal geometry provides a somewhat larger area with fullfold coverage than brick and slanted geometry. Also the OVT gathers have better behaving edges for orthogonal geometry than for the other two geometries.

In summary, brick geometry only scores better than orthogonal geometry for LMOS, whereas slanted geometry has this same advantage over orthogonal geometry. Slanted geometry provides better imaging than brick geometry because of the better spatial continuity. Orthogonal geometry scores best for imaging and for efficiency, whereas it matches slanted geometry with respect to noise removal.

The brick geometry discussed in this paper is (was) the most common implementation of staggered shot lines. Another implementation is the triple stagger in which only one-third of each shot line is sampled with actual shots. In my view using triple stagger does not serve any useful purpose.

Conclusions

This study has shown that LMOS of brick geometry is about 12.5 % smaller than the LMOS of the equivalent orthogonal geometry, not as big a difference as often thought. Slanted geometry has the same LMOS advantage as brick geometry. These advantages become less important with smaller line intervals.

It turns out that singlefold OVT gathers are also possible in brick geometry with even better imaging results than with equivalent OVT gathers of orthogonal geometry. However, the combination of reciprocal OVTs (which is always possible in the fullfold area of a center-spread geometry) produces considerably better results with orthogonal geometry than with brick geometry. Imaging of slanted geometry using reciprocal OVTs is better than brick geometry but worse than orthogonal geometry.

A major advantage of orthogonal geometry and slanted geometry over brick geometry is the continuity in the cross-spread and slanted spread which allows much better coherent-noise removal than in the discontinuous cross-spread of brick geometry.

With respect to implementation of the geometries in the field, orthogonal geometry is more efficient than slanted and brick geometry.

All in all, this paper does not provide any reason to change earlier recommendations not to use brick or slanted geometry.

This paper has also confirmed earlier results reported in Vermeer (2012) that optimal acquisition requires regular geometry with center-spread configurations. One-sided (only two quadrants of each cross-spread) acquisition is suboptimal as it does not provide reciprocal OVTs and it tends to produce a more serious acquisition footprint, also after imaging. An alternative is to use very small line intervals to reduce the sparsity of the geometry.

References

Jianming, T., H. Yue, X. Xiangrong, J. Tinnin, and J. Hallin, 2009, Application of converted-wave 3D/3-C data for fracture detection in a deep tight-gas reservoir: The Leading Edge, **28**, no. 7, 826–837.

Karagül, A., R. Crawford, J. Sinden, and S. Ali, 2004, Recent advances in 3D land processing: Examples from the Pakistan Badin area, First Break, **22**, no. 9, 37-40.

Konyushenko, A., V. Shumilyak, V. Solgan, A. Inozemtsev, V. Solovyev, and Z Koren, 2014, Using full-azimuth imaging and inversion in a Belarus salt dome tectonic regime to analyze fracturing in Upper Devonian intersalt and subsalt carbonate reservoirs: First Break, **32**, no. 9, 81-88.

Vermeer, G. J. O., 1994, 3-D symmetric sampling: 64th Annual International Meeting, SEG, Expanded Abstracts, 906-909.

Vermeer, G. J. O., 1998, 3-D symmetric sampling: Geophysics, **63**, no. 5, 1629–1647.

Vermeer, G. J. O., 2012, 3-D seismic survey design, second edition, SEG.

Acknowledgement

Figures 2, 4, 6, 7b, 7c, 9, 10, and A2 were made with Omni 3D.

Appendix A LMOS in brick geometry

For the derivation of a good approximation of LMOS in brick geometry, I assume equal shot line interval and receiver line interval with SLI = RLI = 2*a*. Figure A1 illustrates this situation. Inside the box with origin *O* in its center the bricked shot line with shots S3 may generate midpoints around the center of the box with absolute offsets smaller than the diagonal of the box (which is representative of LMOS for an orthogonal geometry that is not bricked). For instance, if S3 would coincide with the upper receiver line, a receiver on the lower receiver line with coordinates (0, -a) would produce a midpoint at O with offset equal to 2a. Yet, this value does not represent the LMOS of the brick geometry.

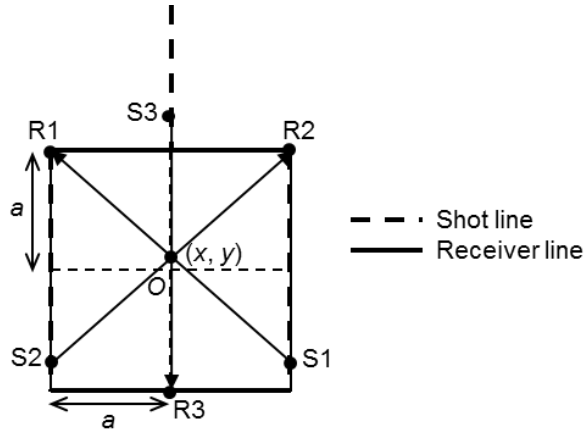

Fig. A1. Derivation of LMOS in brick geometry.

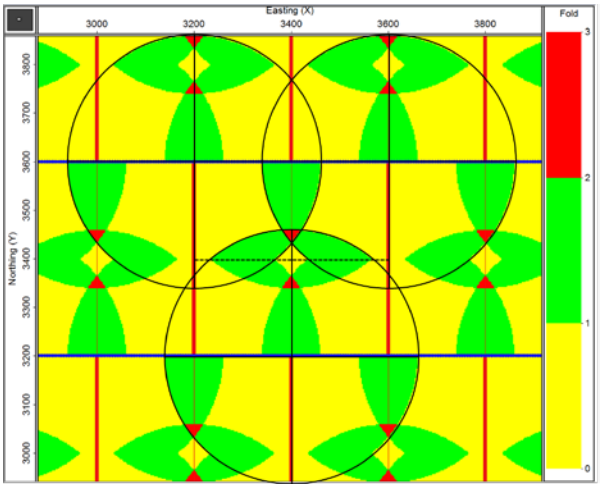

Fig. A2. Fold map for absolute offsets < 520 m in brick geometry with 5-m sampling and LMOS = 500 m. Circles with 520-m diameter.

To determine LMOS of the brick geometry it helps to realize that the cross-spread of a partially sampled shot line consists of a number of narrow strips with crossline dimension *a* (see Figure 3 in main text). So, let us investigate the midpoints in the upper part of the box in Figure A1. The three cross-spreads with center at R1, R2, and R3 provide midpoints to this strip. The midpoints having equal offset LMOS are located on three circles with their centers in R1, R2, and R3 and with radius LMOS/2. Because of symmetry circles with center in R1 and R2 always intersect along line *x* = 0. See also Figure A2, which shows three circles with radius > LMOS/2. The upper part of the small central yellow area with fold 1 (above horizontal black line) consists of midpoints provided by the lower circle.

So, we have to find the intersection of three circles in one point with formulas

$$\text{offset1} = 2\sqrt{(x+a)^2 + (y-a)^2}$$

$$\text{offset2} = 2\sqrt{(x-a)^2 + (y-a)^2}$$

$$\text{offset3} = 2\sqrt{x^2 + (y+a)^2}$$

or LMOS = offset1 = offset2 = offset3, where *x* = 0. For (*x*, *y*) = (0, a/4), offset1 = offset2 = offset3 = 5a/2 = 1.25 RLI. This value is really the largest minimum offset in the brick geometry. It is still 13% smaller than LMOS = 2a√2 for orthogonal geometry, but not as much as suggested in Vermeer (1998).

The above derivations were made assuming infinitely small shot and receiver sampling intervals. In practice, using realistic sampling, the actual LMOS are smaller than the ones derived here.

Appendix B LMOS in slanted geometry

For the derivation of a good approximation of LMOS in slanted geometry, I assume equal shot line interval and receiver line interval with SLI = RLI = 2a. Figure B1 illustrates this situation. The box with origin *O* in its center is diamond-shaped this time. In the two halves of the box on either side of the long diagonal there are now three slanted spreads that may provide the largest minimum offset. In the lower right half the slanted spreads at the lower-left edge, the lower right edge and the upper-right edge may contribute. For each slanted spread a shot-receiver pair is indicated with its midpoint at (x, y).

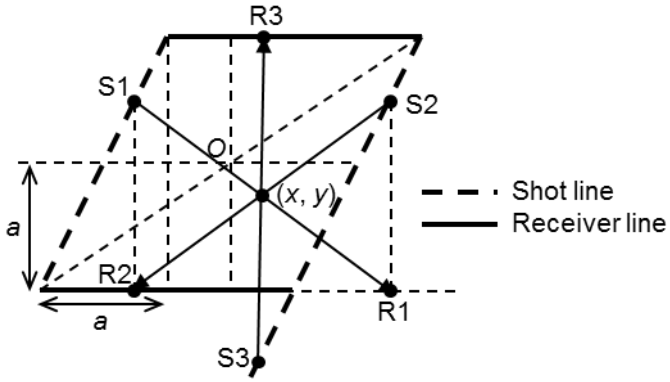

Fig. B1. Derivation of LMOS in slanted geometry.

To determine LMOS of the slanted geometry we first compare shot receiver combinations (S1, R1) with (S2, R2) that share the same midpoint (*x*, *y*). Then we have S1 (*y* – *a*/2, 2*y* + *a*), R1 (2*x* – *y* + *a*/2, - *a*) and S2 (*y* + 3*a*/2, 2*y* + *a*), R2 (2*x* – *y* – 3*a*/2, -*a*) with

$$\text{offset1} = \sqrt{(2x - 2y + a)^2 + (2y + 2a)^2}$$

$$\text{offset2} = \sqrt{(2x - 2y - 3a)^2 + (2y + 2a)^2}$$

where offset1 and offset2 are the corresponding absolute offsets. Note that the offset formulas represent ellipses for slanted geometry. Note also that the y-components of the two offset vectors S1R1 and S2R2 are the same. We find that offset1 = offset2 along line l: *x* - *y* = *a*/2. In the third slanted spread we have S3 (*y* + *a*/2, 2*y* – *a*) and R3 (2*x* – *y* – *a*/2, *a*) with

$$\text{offset3} = \sqrt{(2x - 2y - a)^2 + (2y - 2a)^2}$$

Setting offset3 = offset1 and using the relation found for offset1 = offset2 we find (*x*, *y*) = (*a*/4, - *a*/4) and offset1 = offset2 = offset3 = 5*a*/2 = 1.25 RLI. This value for LMOS happens to be the same as for the brick geometry.

Substituting the derived value for (x, y) into the coordinates of the three offset vectors we find S1 (- 3*a*/4, *a*/2), R1 (5*a*/4, -*a*), S2 (5*a*/4, *a*/2), R2 (-3*a*/4, -*a*), and S3 (*a*/4, -3*a*/2), R3 (*a*/4, *a*). Note that the *x*-coordinates of S3 and R3 are the same.

The above derivations were made assuming infinitely small shot and receiver sampling intervals. In practice, using realistic sampling, the actual LMOS are smaller than the ones derived here.